

Near-field autocorrelation spectroscopy of disordered semiconductor quantum wells

Christoph Lienau, Francesca Intonti,* Tobias Guenther, and Thomas Elsaesser

Max-Born-Institut für Nichtlineare Optik und Kurzzeitspektroskopie, Max-Born-Straße 2A, D-12489 Berlin, Germany

Vincenzo Savona

Institute of Theoretical Physics, Swiss Federal Institute of Technology Lausanne, CH-1015 Lausanne EPFL, Switzerland

Roland Zimmermann

Institut für Physik, Humboldt-Universität zu Berlin, Newton-Straße 15, D-12489 Berlin, Germany

Erich Runge

Max-Planck-Institut für Physik komplexer Systeme, Nöthnitzer-Straße 38, D-01187 Dresden, Germany

(Received 10 July 2003; revised manuscript received 10 October 2003; published 10 February 2004)

Spatially resolved photoluminescence spectra of thin GaAs quantum wells are measured by near-field spectroscopy, and two-energy autocorrelation functions of the spectra are derived. We demonstrate distinctly different autocorrelation functions for a 3-nm-thick quantum well grown on a (311)A surface and for quantum wells grown on (100) substrates. The autocorrelation spectra of the (311)A GaAs quantum well are quantitatively described by a statistical disorder model with a single correlation length of 17 nm for the exciton center-of-mass motion. A shoulder in the autocorrelation spectrum at energies between 1 and 3 meV is identified as a signature of excitonic level repulsion in the disorder potential. In contrast, the characteristic feature in the autocorrelation spectra of the (100) quantum wells is an additional positive correlation peak at energies between 3 and 4 meV. This peak reflects the energy correlations between ground and excited exciton states in individual monolayer islands with a narrow size distribution. The results indicate that the disorder potential in these high-quality (100) GaAs quantum wells contains both contributions from monolayer islands and nano-roughness on a length scale of the exciton Bohr radius.

DOI: 10.1103/PhysRevB.69.085302

PACS number(s): 78.67.De, 78.55.Cr, 07.79.Fc

I. INTRODUCTION

Recently, there has been considerable experimental¹⁻⁷ and theoretical interest^{8,9} in studying the effects of excitonic level repulsion in disordered semiconductor nanostructures, e.g., narrow quantum wells and wires. In such systems, interface roughness and alloy fluctuations on a nanometer scale lead to spatial variations in the effective excitonic center-of-mass potential that tend to localize the excitonic wave functions. This localization gives rise to inhomogeneously broadened macroscopic photoluminescence (PL) spectra. In experiments with high spatial and spectral resolution, however, the inhomogeneously broadened spectra break up into narrow emission spikes from single localized excitons. Despite the random nature of the disorder potential, the exciton emission energies are correlated in such local spectra. Whenever the wave functions of nearly isoenergetic exciton states are spatially overlapping, quantum mechanical level repulsion¹⁰ is expected to occur. As a result, energy differences between the emission spikes in the local spectra that are smaller than the energy splitting associated with level repulsion become unlikely.

In disordered semiconductors, the exciton emission energies are well described as eigenenergies of a static Schrödinger equation.^{11,12} It was predicted a few years ago that the ensemble-averaged autocorrelation function of near-field PL spectra is sensitive to level repulsion.⁸ Experimentally, such correlation functions have first been reported for a disordered GaAs quantum well (QW).¹³ A small dip at energy differ-

ences of 100 μeV in the autocorrelation function was considered to be consistent with the observation of level repulsion. PL autocorrelation functions of near-field spectra from CdSe/ZnSe layers² showed a clear positive correlation feature. Its energy position is consistent with the splitting between ground and excited states in the same local potential minimum. Hence, the peak was assigned to quantization within rather uniform islands.

In Ref. 1, we quantitatively compared experimental near-field PL autocorrelation spectra from a (311)A GaAs QW to a theoretical analysis assuming a statistical disorder potential with a correlation length of 17 nm. Based on the excellent agreement between experiment and model, a shoulder in the autocorrelation function at energies between 1 and 3 meV was identified as evidence for level repulsion.

This interpretation was recently questioned on the basis of measurements with (100) GaAs QWs.³ Near-field autocorrelation spectra from such samples showed a peak around 3 meV. The experimental results and data modified by energy filter functions were compared to one-dimensional model simulations. It was concluded that the 3-meV peak in the autocorrelation is not related to level repulsion predicted for a statistical disorder potential with a single correlation length. Recently, autocorrelation spectra from disordered quantum wires⁵ have been interpreted as being consistent with the predicted level repulsion scenario.

Many of the experimental results obtained on the different samples contain features that are not yet well described by the currently available models for statistical disorder poten-

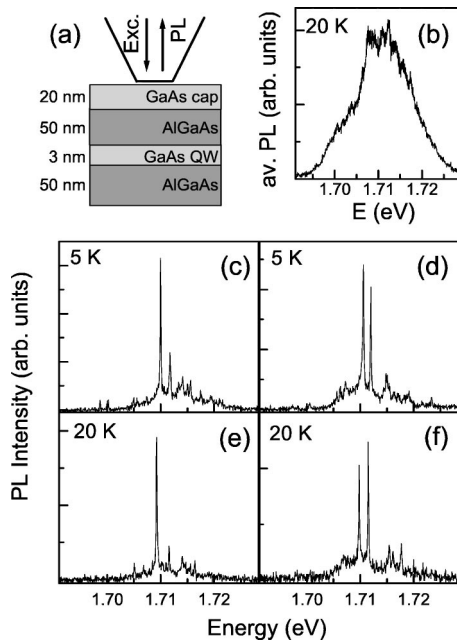


FIG. 1. (a) Schematic experimental setup. (b) Averaged PL spectrum ($T=20$ K) of the 3-nm (311)A GaAs QW. (c) and (d) Representative near-field PL spectra of that sample recorded at 5 K at two different spatial positions. (e) and (f) Near-field PL spectra recorded at 20 K at the same positions of (c) and (d), respectively (Ref. 1).

tials with single correlation lengths.^{8,9} This fact raises the question as to what extent near-field autocorrelation spectra can provide quantitative information about these potentials. This problem can be addressed by comparing autocorrelation spectra from samples where independent information on the disorder is available. For instance, atomically almost flat monolayer islands exist in high-quality single GaAs quantum wells grown with growth-interruption on (100) substrates. The island dimensions can reach more than 100 nm, much larger the exciton Bohr radius.^{14,15} In addition, nanoroughness exists on a length scale smaller than the exciton diameter and a bimodal roughness model¹⁶ is the simplest model that can account for this behavior.

In this paper, near-field autocorrelation spectra from (311)A GaAs and (100) GaAs quantum wells are compared. We demonstrate a distinctly different behavior of such two types of samples: For (311)A GaAs quantum well, the autocorrelation spectra are well described by a statistical disorder model with a single correlation length. For (100) GaAs quantum wells, we observe an additional pronounced positive correlation peak at energies around 3–4 meV. This peak is not reproduced by statistical models assuming a single correlation length. We assign this peak to correlations between excitonic eigenstates in single monolayer islands of similar shape and size.

II. EXPERIMENT

We investigate two different QW samples. One is a GaAs/AlGaAs quantum well grown by molecular beam epitaxy (MBE) on a GaAs (311)A substrate.¹⁷ It consists of a single 3-nm-thick GaAs QW layer clad between two 50-nm-thick

$\text{Al}_{0.5}\text{Ga}_{0.5}\text{As}$ barrier layers and capped with 20 nm of GaAs [Fig. 1(a)]. The other sample consists of 12 single QW layers of different thickness grown on a (100) GaAs substrate. The QW layers are separated by AlAs/GaAs short period superlattice barriers, each formed by nine AlAs and GaAs layers with a total thickness of 23.8 nm. Here, we investigate the top four QWs with thicknesses of 3.3, 4.0, 4.5 and 5.1 nm. The layers are buried at distances of 40, 67.1, 94.9, and 123.2 nm below the surface. Growth interruptions of 10 s at each interface lead to a large correlation length of the QW disorder potential and to the formation of interface quantum dots. The growth interruptions are kept short in order to avoid a monolayer splitting of the macroscopic PL spectra and to minimize incorporation of impurities at the interfaces.

A low-temperature near-field scanning optical microscope¹⁸ is used in an illumination/collection geometry with a combined spatial and spectral resolution of 150 nm and 100 μeV [Fig. 1(a)]. In this geometry, the sample is excited with light from a HeNe laser (1.96 eV), transmitted through a chemically etched, uncoated near-field fiber probe.¹⁹ Photoluminescence from the sample is collected through the same probe, dispersed in a $f=50$ cm monochromator and detected with a cooled charge-coupled device. Near-field PL spectra are recorded by scanning the fiber probe across the sample surface. At each tip position, spectra are integrated for approximately 0.5 s.

III. RESULTS

The spatially averaged PL spectrum of the (311)A GaAs QW at $T=20$ K shows a 15-meV broad emission band [Fig. 1(b)]. The spectrum is obtained by averaging over 432 individual spectra recorded by scanning a $1.2 \times 3.6\text{-}\mu\text{m}^2$ area with steps of 100 nm. Such sets of near-field spectra are taken at temperatures between 5 and 30 K at steps of 5 K and for different excitation powers between 100 nW and 4 μW coupled into the near-field fiber probe. In contrast to the averaged emission, the individual near-field spectra break up into a series of spectrally sharp and intense emission lines. Representative near-field PL spectra recorded at a fixed spatial position are displayed in Figs. 1(c)–1(f) for temperatures of 5 and 20 K. In this range of powers, the shape of the PL spectra is not affected by variations of the excitation intensity and the emission intensity of the sharp spikes varies linearly with excitation power.¹ This shows that the spectrally sharp emission spikes originate from single localized excitons within the QW disorder potential. The spatial extension of the individual spikes is limited by our spatial resolution of 150 nm.²⁰ We have carefully studied intensity-dependent near-field spectra. The intensity of the individual emission lines depends linearly on the excitation density and we do not observe the appearance of new emission lines at higher excitation densities.¹ This rules out that these emission lines arise from biexcitonic transitions²¹ and makes contributions from charged excitons²² unlikely. We therefore believe that such transitions have only a minor effect on the autocorrelation spectra discussed below.

Similar sets of near-field PL spectra were recorded for the set of (100) quantum wells (lattice temperature $T=12$ K).

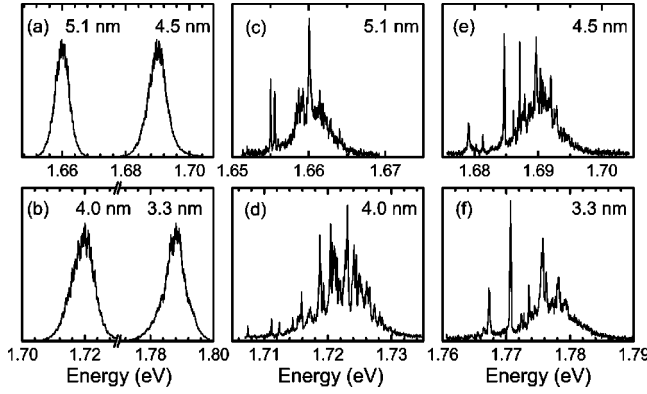


FIG. 2. PL spectra of the (100) GaAs quantum wells at $T = 12$ K. (a) Averaged PL spectrum of the 3.3- and 4.0-nm QWs. (b) Averaged PL spectrum of the 4.5- and 5.1-nm QWs. (c)–(f) Representative near-field PL spectra recorded at an excitation power of 110 nW of the 5.1- (c), 4.0- (d), 4.5- (e), and 3.3-nm (f) QWs, respectively.

Here, for each QW and excitation intensity, 900 near-field spectra are recorded by scanning a $9 \times 9\text{-}\mu\text{m}^2$ area with steps of 300 nm. The spatially averaged PL spectra [Figs. 2(a) and 2(b)] for the 4.0- to 5.1-nm-thick QWs show a 5–9-meV broad emission line, which is well described by a Gaussian shape.¹¹ Slight deviations from a Gaussian shape are seen for the thinnest QW (3.3 nm). We note that the far-field PL spectra of these samples show no indication for a monolayer splitting of the PL line. In Figs. 2(c)–2(f), representative near-field PL spectra are shown which were recorded with an excitation intensity of 110 nW, corresponding to an average excitation density well below one exciton per monolayer island. For excitation powers between 1 and 500 nW, we find a linear intensity dependence and an excitation-independent shape of the emission spectra, indicating negligible contributions from biexcitons and charged excitons. In general, the near-field spectra of these samples show a larger number of sharp spikes and a more intense, spectrally broad background emission^{20,23} than those taken on the (311)A GaAs QW.

We now present near-field autocorrelation spectra of these samples. Two-energy *autocorrelation functions*

$$R_c(\Delta E) = R(\Delta E) - R_0(\Delta E) \quad (1)$$

are calculated as outlined in Ref. 1 by taking the difference between the ensemble-average over the autoconvolution of individual near-field spectra,

$$R(\Delta E) = \left\langle \int dE' I_n(E') I_n(E' - \Delta E) \right\rangle, \quad (2)$$

and the autoconvolution of the ensemble-averaged near-field spectra,

$$R_0(\Delta E) = \int dE' \langle I_n(E') \rangle \langle I_n(E' - \Delta E) \rangle. \quad (3)$$

Here, $I_n(E)$ represents the n th local optical spectrum taken on the sample under investigation, and $\langle \dots \rangle$ denotes the ensemble average over many individual measurement spots.

Figure 3 shows experimental autocorrelation functions

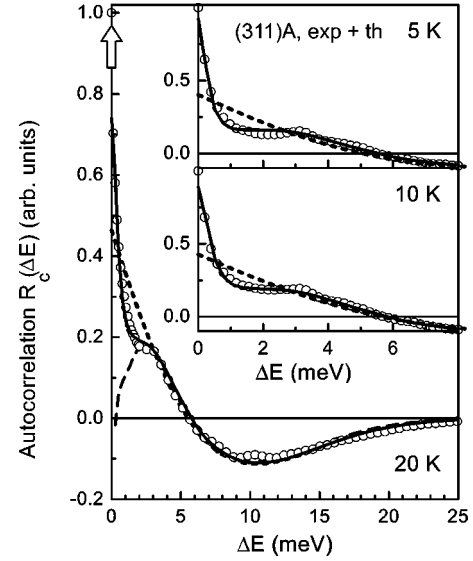


FIG. 3. Autocorrelation function $R_c(\Delta E)$ at $T=20$ K, shown for the experimental data on the (311)A GaAs QW (circles), the numerical simulation (solid line), the classical limit (dotted line) and the numerical simulation without the self-correlation peak (dashed line). Level repulsion is evident from the deviation between the experimental data and classical limit at energies below 3 meV. The arrow denotes the δ -function part (self-correlation) of the dashed curve. Insets: autocorrelation functions at $T=5$ and 10 K, respectively.

$R_c(\Delta E)$ measured with the 3-nm-thick (311)A GaAs QW at three different temperatures. $R_c(\Delta E)$ is normalized to unity at $\Delta E=0$. The main features of $R_c(\Delta E)$ are (i) a sharp self-correlation peak around $\Delta E=0$, (ii) a clear shoulder visible at energies between 1 and 3 meV, and (iii) for higher energies, a behavior that is expected from classical theory: $R_c(\Delta E) > 3$ meV decreases monotonically, becomes negative, and reaches a minimum at $\Delta E \approx 10$ meV. Then it increases again and approaches zero around 25 meV, i.e., about twice the linewidth of the averaged PL spectrum. For $T < 20$ K, the autocorrelation functions are almost independent of temperature. In particular, the energy range of the level repulsion signature around 1–3 meV and the zero crossing in $R_c(\Delta E)$ remain unaffected [Fig. 3 (inset)]. There is no peak in $R_c(\Delta E)$ around 3 meV, as erroneously claimed in Ref. 3. At 25 K (not shown), the level repulsion signature in the data is clearly less pronounced. At 30 K, the linewidth of the individual sharp spikes increases and their contribution to the total spectrum decreases, preventing a meaningful analysis of $R_c(\Delta E)$.

The autocorrelation functions derived from the spectra of the (100) GaAs QWs (Fig. 4) are strikingly different. For all QWs, a very sharp self-correlation peak with a width of about 0.2 meV is observed. Outside the self-correlation peak, R_c first decreases and then shows a clear correlation peak at energies around 3 and 4 meV. At higher energies, R_c reaches a minimum with a negative value of R_c at energies between 4 meV (5.1 nm) and 6.5 meV (3.3 nm). Zero is approached at energies between 10 meV (5.1 nm) and 15 meV (3.3 nm). The energy position of the additional correlation peak red-

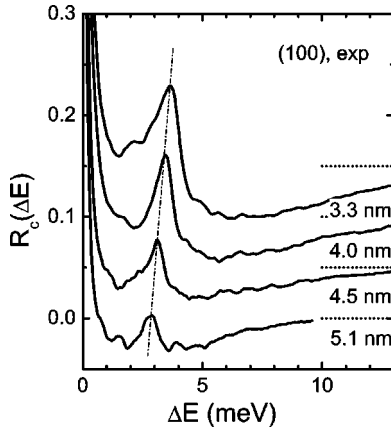


FIG. 4. Autocorrelation function $R_c(\Delta E)$ of four different growth-interrupted (100) GaAs QWs at $T=12$ K. The QW thicknesses are 3.3, 4.0, 4.5, and 5.1 nm. For clarity, the curves are each shifted by 0.05 in the vertical direction. The correlation peak around 3–4 meV is a signature of the correlation between ground and excited state PL of excitons localized in the same island.

shifts with increasing well thickness from 3.6 meV (3.3 nm) to 2.8 meV (5.1 nm). For excitation powers ≤ 500 nW, these autocorrelation functions are insensitive to the excitation intensity, as is shown for the 3.3-nm QW in Fig. 5.

IV. DISCUSSION

A quantitative analysis of the near-field autocorrelation spectra requires a careful line shape analysis. We compare these data to a statistical analysis of excitonic spectra in disordered nanostructures. The spectrally sharp emission spikes in the near-field originate from single excitons which are localized within the quantum well disorder potential caused by interface roughness and alloy fluctuations. We assume that the disorder-induced energy fluctuations are not larger than the exciton binding energy and that the relative electron-hole motion is undistorted by the disorder.¹¹ The excitonic center-of-mass (COM) wave function then obeys a

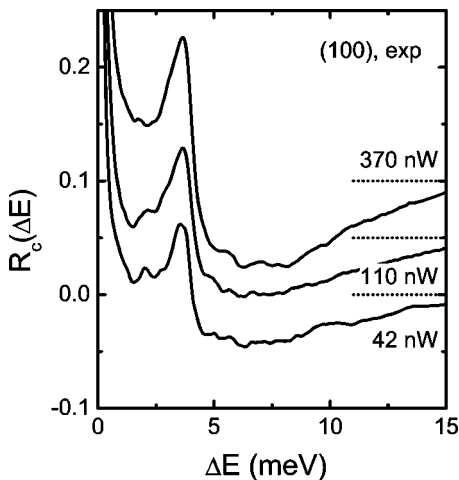


FIG. 5. Excitation-intensity-dependent autocorrelation functions $R_c(\Delta E)$ of the 3.3-nm-thick (100) GaAs QW at $T=12$ K. The spectra are recorded at excitation powers of 42, 110, and 370 nW.

TABLE I. The parameters used in the simulation for the 3-nm 311(A) GaAs QW and the experimental values of the homogeneous linewidth Γ_{expt} .

	σ (meV)	Γ (meV)	Γ_{expt} (meV)
5 K	5.1	0.15	0.18 ± 0.02
10 K	5.3	0.18	0.20 ± 0.03
20 K	5.3	0.22	0.19 ± 0.03

two-dimensional Schrödinger equation with an effective disorder potential $V(\mathbf{R})$. The latter is given by the convolution of the $1s$ -exciton wave function with the local quantum well band edge fluctuations, i.e., the exciton relative motion averages over potential fluctuations on a length scale determined by an exciton Bohr radius of 7–10 nm. In our simulations, we model the effective potential $V(\mathbf{R}) \propto \int \exp(-|\mathbf{R}-\mathbf{R}'|/\xi) U(\mathbf{R}') d\mathbf{R}'$ as the convolution of a spatially uncorrelated white noise function $U(\mathbf{R})$ with an exponential function $\exp(-|\mathbf{R}|/\xi)$. The average potential amplitude is $\sigma^2 = \langle [V(0)]^2 \rangle$. The spatial correlation length ξ of the potential is taken as an adjustable parameter. A minimum value for ξ is given by the exciton Bohr radius. As pointed out before,⁹ the ensemble-averaged properties of the Schrödinger equation do not depend independently on ξ and σ but only on the ratio σ/E_c , where $E_c = \hbar^2/(2M\xi^2)$ is a natural energy unit for the COM confinement (M is the exciton mass).⁹

In the numerical simulations, eigenvalues ϵ_α and eigenvectors ψ_α of the two-dimensional Schrödinger equation are calculated for 1000 random realizations of the disorder potential $V(\mathbf{R})$. The simulations are performed using periodic boundary conditions on a grid of 32×32 points with a step size of $\xi/4$. For each excitonic COM eigenstate α the optical matrix element is calculated as $M_\alpha = \int \psi_\alpha(\mathbf{R}) d\mathbf{R}$. The local absorption spectrum for a single spot n is taken as

$$D_n(E) = \frac{1}{A} \sum_{\alpha} M_{\alpha,n}^2 \delta(E - \epsilon_{\alpha,n}), \quad (4)$$

where A is the spot area.¹

Autocorrelation functions $R_c(\Delta E)$ are simulated from the calculated absorption spectra using Eqs. (1) and (2) by performing ensemble averages over the different realizations of the disorder potential. The parameters σ and ξ of the disorder potential are obtained by fitting the computed $R_c(\Delta E)$ to the experimental data. To account for the finite linewidth in the experimental spectra, R_c is convoluted with a Lorentzian of width 2Γ .

We first discuss the results for the (311)A QW. Figure 3 compares the computed and the experimental functions $R_c(\Delta E)$. The main panel shows the experimental result at 20 K and the corresponding full simulation including Lorentz convolution. We achieve good agreement for the parameters given in Table I, i.e. for a correlation length of $\xi = 17$ nm, for $\sigma = 5.1$ meV, and $\Gamma = 0.22$ meV. The value of Γ mainly defines the width of the self-correlation peak around $\Delta E = 0$ and is in good agreement with an average linewidth of $\Gamma = 0.19 \pm 0.03$ meV of the individual localized exciton spikes in the near-field spectra. The simulations reproduce the

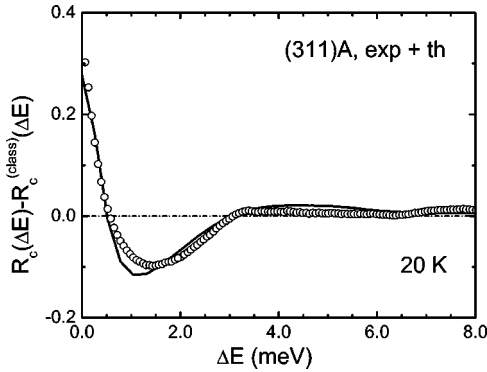


FIG. 6. Difference between $R_c(\Delta E)$ at $T=20$ K and the classical autocorrelation $R_c^{(\text{class})}(\Delta E)$ for the (311)A GaAs sample [Fig. 3]. The experimental data are shown by circles and the numerical result by a solid line. The level repulsion effect gives rise to *negative* values of $R_c(\Delta E) - R_c^{(\text{class})}(\Delta E)$.

shoulder in $R_c(\Delta E)$ between 1 and 3 meV, which we identify as the signature of the quantum mechanical level repulsion in this sample. Also for larger energies $\Delta E > 3$ meV, the simulation reproduces the experimental line shape. In this energy range, the line shape is entirely given by the energy correlation function of the disorder potential. The agreement between the experimental data and the quantum-mechanical result is equally satisfying for the data taken at $T=5$ K and $T=10$ K on the same sample region (insets in Fig. 3). For these fits, σ and Γ had to be slightly adjusted (Table I).

To interpret these results, it is helpful to compare them to two additional simulations, (i) a calculation of the classical correlation function and (ii) a calculation neglecting the self-correlation. In the “classical” limit, i.e., for an exciton kinetic energy that is negligibly small compared to the disorder potential energy (the limit $\hbar \rightarrow 0$), the eigenvalues of the Schrödinger equation are simply given by the local values of $V(\mathbf{R})$. In this limit, $R_c^{(\text{class})}(\Delta E)$ still takes on finite values. In potentials with finite correlation lengths, it is more likely to find similar values of $V(\mathbf{R})$ in the immediate vicinity and hence $R_c^{(\text{class})}(\Delta E)$ is positive at small energy values. This positive correlation is compensated for by negative values of $R_c^{(\text{class})}(\Delta E)$ at large energy differences, and the integral $\int R_c^{(\text{class})}(\Delta E) dE$ vanishes. For a given form of the potential, an analytical expression for $R_c^{(\text{class})}(\Delta E)$ can be derived, which is included in Fig. 3. At all temperatures, this classical autocorrelation is in good agreement with the experiments at energies $\Delta E > 3$ meV. The effect of the finite exciton kinetic energy is a level splitting of exciton states with spatially overlapping wave functions. Due to this level repulsion, energy splittings with small values of ΔE are less likely than predicted by the classical autocorrelation function. Thus the level repulsion effect shows up in $R_c(\Delta E) - R_c^{(\text{class})}(\Delta E)$ as a distinct negative dip. This level repulsion dip is clearly seen in both experimental and theoretical data for energies $\Delta E < 3$ meV (Fig. 6). This energy *anticorrelation* is compensated for by the spectrally narrow positive self-correlation peak around $\Delta E = 0$. It arises from the self-convolution of the individually sharp emission spikes in the near-field PL spectra. Its width is roughly twice the linewidth of the sharp

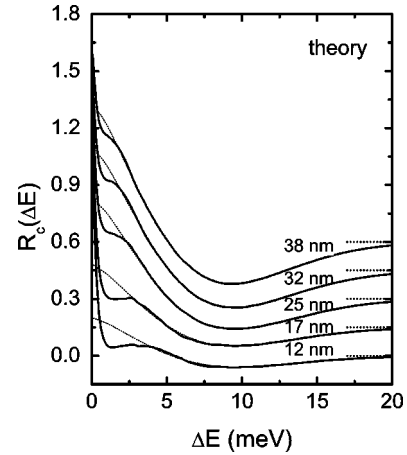


FIG. 7. Simulated autocorrelation functions $R_c(\Delta E)$ as a function of correlation length ξ for fixed values of $\sigma = 5.3$ nm and $\Gamma = 0.15$ meV. The dotted lines show the classical correlation function. The curves are vertically shifted by 0.15.

PL spikes. The slight increase in width with temperature reflects the broadening of the exciton peaks due to the scattering with acoustic phonons.¹⁴ We consider the satisfactory agreement between experimental and theoretical results direct evidence of quantum mechanical level repulsion in disordered semiconductor nanostructures.

In Figs. 3 and 6, we have compared theoretical correlation functions calculated from absorption spectra to data taken from PL experiments. This seems valid only if the effective temperature of the exciton gas is larger than the energy separation between neighboring localized states. In previous experiments²⁰ on the quantum wire region of the same sample, we estimated an effective exciton temperature of at least 30–40 K to explain the strong PL emission from delocalized exciton states at higher energies. Theoretical studies of exciton kinetics in QWs with interface roughnesses of similar magnitudes also indicate that at low temperatures the exciton distribution differs significantly from a Boltzmann distribution in equilibrium with the lattice temperature. This is in agreement with conclusions drawn from recent time-resolved photoluminescence experiments.²⁴ Thus, the comparison of correlation functions from absorption and PL data is at least qualitatively justified. For a full quantitative analysis, a theoretical description including exciton relaxation processes is needed.^{25,26} Additionally, autocorrelation functions measured using recently established nonlinear optical techniques^{15,27} shall provide further insight. We expect that population effects in PL-based autocorrelation functions will mainly change the values σ for the strength of the disorder potential. This is suggested by the slight adjustment of σ (Table I) necessary to reproduce the temperature dependent measurements.

The correlation length ξ affects primarily the small energy part of R_c . This is seen in Fig. 7, comparing simulated $R_c(\Delta E)$ curves for different values of ξ , while keeping $\sigma = 5.3$ meV and $\gamma = 0.22$ meV constant. For large values of ξ , $\sigma/E_c \rightarrow 0$ and R_c approaches the classical correlation function $R_c^{(\text{class})}(\Delta E)$. For small values of ξ , the level repulsion anticorrelation becomes more pronounced. Since the ef-

fective disorder potential $V(\mathbf{R})$ is given as a convolution between the microscopic disorder potential and the exciton wave function for relative electron-hole motion, the minimum value of ξ that can be realized in semiconductor nanostructures is given by the exciton Bohr radius. Thus the “white noise” limit, $\sigma/E_c \rightarrow 0$ cannot be fully reached. Figure 7 shows that R_c depends quite sensitively on ξ and that a quantitative comparison between experimental and calculated correlation functions allows to extract the value of the correlation length with reasonable accuracy. In the case of the (311)A GaAs QW, we estimate $\xi = 17_{-3}^{+8}$ nm.

This interpretation of the level repulsion dip in the autocorrelation function was recently questioned.³ In Ref. 3, near-field autocorrelation spectra on (100) GaAs QWs recorded under similar experimental conditions are discussed. The experimental autocorrelation functions are similar in shape to those calculated for a one-dimensional disorder model without monolayer islands. When multiplying the experimental and simulated spectra by filter functions of the form

$$f(E) \propto \exp(E/E_0), \quad (5)$$

with a filter parameter E_0 , however, a different behavior was found for experimental and theoretical autocorrelation functions. Based on these findings, the authors concluded that a 3-meV peak in their autocorrelation functions is not consistent with level repulsion.

The authors of Ref. 3 motivated the use of such filter functions by their expectation that the level repulsion effect should be more pronounced for the spatially more extended high-energy levels in the optical spectra. Recent one-dimensional simulations of energy-resolved autocorrelation functions demonstrate that this hypothesis is oversimplified.²⁸ At low energies, the localization length decreases and the energy splitting between overlapping states can be large. At higher energies, the density of states increases but the states are spatially more extended and thus the splitting is reduced.²⁰ Also, the damping of the exciton resonances from spatially extended states due to phonon emission is strong. Therefore, individual exciton resonances from spatially extended states are generally not observed and the emission from these states mostly appears a broad continuum,²⁰ representing a superposition of many different exciton resonances. This makes it difficult to observe level repulsion at higher energies. As a result, the use of filter function is not appropriate for deciding on level repulsion.

This conclusion is further supported by applying filter functions to the experimental and theoretical data in Fig. 3. As previously observed,³ the filter function strongly deforms the autocorrelation curves. In the case of the (311)A GaAs QW studied in this work, their influence on experimental data and simulation results is qualitatively similar. Figure 8 shows theoretical simulations for $\sigma = 5.3$ meV, $\xi = 17$ nm, and $\Gamma = 0.15$ meV. The data are compared to simulations of the classical correlation functions $R_c^{(\text{class})}(\Delta E)$ (dotted lines).²⁹ For comparison with experiment (Fig. 9), an energy range of 20 meV around the center of the absorption spectrum is analyzed. Two features are most pronounced: (i) the

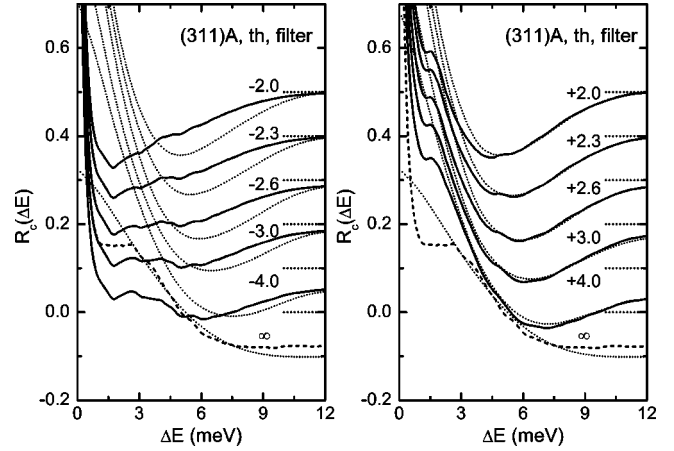


FIG. 8. Simulated autocorrelation functions $R_c(\Delta E)$ for $\xi = 17$ nm, $\sigma = 5.3$ nm and $\Gamma = 0.15$ meV. $R_c(\Delta E)$ are shown for different filter functions $f(E) = \exp(E/E_0)$ multiplied by the individual near-field PL spectra. The curves are vertically shifted for clarity by 0.1 and the filter parameter E_0 is indicated. The autocorrelation of the raw data is included by a dashed line. It corresponds to $E_0 \rightarrow \infty$. The dotted lines show the classical correlation functions for the different values of E_0 .

shoulder in the experimental data, i.e., the signature of level repulsion in our data, is smeared out if the filter parameter E_0 becomes similar to or smaller than the energy range over which the level repulsion signature extends. The shoulder around 1–3 meV vanishes for both positive *and* negative values of E_0 . For small negative values of E_0 the strong self-correlation peak persists and there is no feature that can be directly assigned to level repulsion. This shows that using such filter functions clearly does *not* enhance the level repulsion feature. (ii) The energetic extent of the “classical” correlation function decreases with decreasing filter parameter.

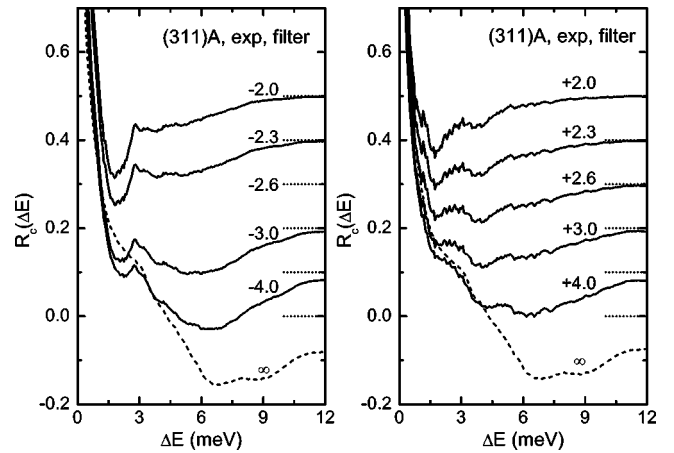


FIG. 9. Experimental autocorrelation spectra $R_c(\Delta E)$ for the 3-nm (311)A GaAs QW ($T = 20$ K), for different filter functions $f(E) = \exp(E/E_0)$ multiplied by the individual spectra. The analysis is limited to energy region from 1.701 to 1.720 meV, around the PL center energy of 1.71 eV. The curves are vertically shifted for clarity by 0.1 and the filter parameter E_0 is indicated. The autocorrelation of the raw data limited to the above given energy region is included as a dashed line. It corresponds to $E_0 \rightarrow \infty$.

This is due to the pronounced spectral reshaping of the optical spectrum for $|E_0| < \sigma$. The filter function $f(E)$ introduces a high energy ($E_0 < 0$) [respectively low energy ($E_0 > 0$)] cutoff of the filtered spectra. Therefore, the energy range of nonzero spectral intensity and the energetic extent of the “classical” correlation function decreases sharply with $|E_0| \rightarrow 0$. This is evident in Fig. 8. A quantitative comparison between $R_c(\Delta E)$ and $R_c^{(\text{class})}(\Delta E)$ as given in Figs. 3, 6, and 7, seems, however, difficult when filter functions are applied. The shape of both functions and also the difference between them depends strongly on the energy range of the spectra that is analyzed. This is due to the strong reshaping of the original spectra by the filter functions and prevents, in our opinion, a physically sound interpretation of these data.

For the experimental spectra, an additional difficulty occurs when filter functions with parameters $|E_0| < 4$ meV are applied. The filter functions vary by several orders of magnitude within the spectral range (approximately 50 meV) covered by the CCD detector and used to calculate the correlation functions. This largely enhances any noise (e.g., CCD dark counts) on the experimental spectra. To minimize such unwanted effects we analyzed only a range of 19 meV around the PL center energy (1.71 eV). Even without filter functions ($E_0 \rightarrow \infty$), this slightly decreased the level repulsion signature (Fig. 9). With the filter functions, the level repulsion signature vanishes for all parameters $|E_0| < 4.0$ meV. The only effect that can clearly be resolved is the narrowing of the energetic range of the classical correlation function. For negative values of E_0 , we note a weak peak around 2.5 meV, which is not present in the unfiltered data at $T = 20$ K. A slight indication of such a peak may also be found in the unfiltered $R_c(\Delta E)$ at $T = 5$ K. While the variation of the filtered experimental autocorrelation function is in qualitative agreement with that seen in the theoretical data, a quantitative comparison seems difficult. The exact shape of the experimental filtered R_c curves depends quite significantly on the energy range of data that is analyzed. We therefore conclude that the use of filter function gives no new reliable information about level repulsion. With and without filter functions, the experimental data for the 3-nm (311)A GaAs QW are in excellent agreement with a disorder model that is based on a single correlation length $\xi \approx 17$ nm.

We now discuss the autocorrelation functions recorded on the (100) GaAs QWs. It is important to recall that the shape of such functions is distinctly different from what is found for the (311)A QWs. In the (100) results, the main characteristic is an additional positive correlation peak at energies E_p between 2.8 and 3.6 meV. The peak energy is much smaller than the monolayer splitting in these samples. This peak is superimposed on a negative correlation feature at higher energies. A dip or shoulder at small energies, related to the level repulsion, however, cannot be resolved. Outside the self-correlation peak, $R_c(\Delta E)$ decreases monotonically for energies smaller than E_p . Such a behavior is clearly not described by statistical disorder models based on a single characteristic length ξ , because these lead to many minima with varying shapes and sizes with ξ describing only average properties. A similar, though less pronounced peak, has re-

cently been observed in autocorrelation functions of CdTe/ZnTe QWs.² It was assigned to the energy correlation between ground and optically active excited exciton states within large, uniform islands. If the energy splitting between these states is similar within a sufficiently large fraction of islands, this *positive* correlation is still present in the ensemble averaged autocorrelation functions. In PL-based experiments, this requires a sufficient population of the excited states.

The correlation between ground and excited states in the same island probably also dominates the autocorrelation functions on our (100) GaAs QWs. The “classical” correlation feature at higher energies then reflects the correlation function due to short-range fluctuations of the disorder potential which are superimposed on the island potentials. One-dimensional simulations of such a two-step disorder model, monolayer islands superimposed on statistical, short-correlation length potential fluctuations, have been successfully used to describe features observed in the autocorrelation functions of single GaAs QWs reported in Ref. 3. A full two-dimensional theory of the exciton optical properties in such a bimodal disorder model is currently not available. Therefore, we cannot yet compare the experimental data in Figs. 4 and 5 to a realistic theoretical disorder model. Also, we cannot include simulations of classical correlation functions in Figs. 4 and 5, which makes a quantitative analysis of the signatures of level repulsion in these spectra difficult.

We have carried out preliminary two-dimensional simulations of autocorrelation functions with such a disorder model. Such calculations indicate that the positive correlation feature found in the experiments cannot be reproduced with a random, statistical distribution of island sizes.³⁰ Only if a narrow size distribution is intentionally chosen, such a feature emerges. In this case, the average extent of these monolayer islands can roughly be estimated from the energy position of the correlation peak. For the 5.1-nm GaAs QW (Fig. 4), the monolayer splitting is about 9.2 meV and the energy of the correlation peak 2.9 meV. Assuming isotropic islands, we estimate an island diameter of about 45 ± 5 nm. This large island diameter agrees quite well with the observed large dipole moments of 50–100 D of these interface quantum dots.^{27,31} The increase of the peak energy E_p with decreasing well width seen in Fig. 4 arises mostly from the increasing monolayer splitting in the narrow wells. Also for the 3.3 to 4.5 nm QWs, similar island diameters of about 45 nm are estimated.

The very different autocorrelation functions in Figs. 3 and 4 are linked to the different surface morphologies of these samples. (311)A GaAs surfaces possess an inherent corrugation with a periodicity of 3.2 nm and a corrugation height of 0.34 nm.³² This interface roughness gives rise to a short-range disorder potential fluctuating on a length scale of about the exciton Bohr radius, even if growth interruptions are employed to smooth the interfaces. High-quality (100) GaAs interfaces, on the other hand, show large atomically almost flat monolayer islands with dimensions of several tens of nanometers.¹⁴ In addition, nanoroughness exists on a length scale smaller than the exciton Bohr radius. Our results indicate that, for such samples, a bimodal disorder model, com-

prising monolayer islands with a narrow size distribution and nanoroughness,^{3,16} is the simplest model that can realistically describe their optical properties.

V. CONCLUSION

In conclusion, we have compared near-field autocorrelation spectra $R_c(\Delta E)$ of a 3-nm (311)A GaAs quantum well and of various thin (100) GaAs quantum wells. The autocorrelation spectra on these samples are markedly different. The results on the (311)A GaAs quantum well are quantitatively described by a two-dimensional statistical disorder model with a single correlation length $\xi = 17$ nm. A shoulder in the autocorrelation spectrum at energies between 1 and 3 meV is identified as a signature of excitonic level repulsion in the disorder potential of the quantum well. At larger energies, the line shape of $R_c(\Delta E)$ is defined by the classical autocorrelation function of the disorder potential. The characteristic feature of autocorrelation spectra of the (100) GaAs quantum wells is an additional positive correlation peak at energies between 3 and 4 meV. This peak reflects the energy correlation between ground and excited exciton states in the same monolayer island. An island size of about 45 nm is estimated. The results indicate that the disorder potential in these samples contains contributions from monolayer islands with a narrow size distribution and nanoroughness on a length scale of the exciton Bohr radius.

The results highlight the sensitivity of near-field autocorrelation spectra to spatial characteristics of the disorder po-

tential. Such autocorrelation spectra reveal by optical means the very different nano-scale disorder in (311)A and (100) GaAs quantum wells. This technique thus presents a promising and powerful technique to analyze disorder effects on the optical properties of semiconductor nanostructures and to obtain information about the underlying disorder potential. For a quantitative analysis, theoretical studies of exciton spectra in bimodal disorder potentials with a small spread of island shapes are required. The experimental results presented in this work and in Refs. 2 and 3 pose to models of MBE growth the challenge to reproduce such interface topologies. Also, the role of exciton population kinetics on autocorrelation spectra deserves further investigation. Important additional information may be obtained from a statistical analysis of spatially resolved linear or nonlinear absorption experiments. Such studies are currently underway.

ACKNOWLEDGMENTS

We thank S. Eshlaghi, A. D. Wieck (University of Bochum), R. Nötzel, and K. H. Ploog (Paul-Drude-Institut, Berlin) for providing the high-quality semiconductor samples. Particular thanks are due to V. Emiliani (Université Paris VI) for important contributions during the initial stage of this work. We gratefully acknowledge support by the Deutsche Forschungsgemeinschaft (SFB296) and the European Union through the EFRE and SQID programs. V.S. acknowledges financial support by the Swiss National Science Foundation through Project No. 620-066060.

*Present address: LENS (Laboratorio Europeo di Spettroscopia non Lineari), I-50019 Sesto Fiorentino (FI), Italy.

¹F. Intonti, V. Emiliani, C. Lienau, T. Elsaesser, V. Savona, E. Runge, R. Zimmermann, R. Nötzel, and K.H. Ploog, *Phys. Rev. Lett.* **87**, 076801 (2001).

²G. von Freymann, E. Kurtz, C. Klingshirn, and M. Wegener, *Appl. Phys. Lett.* **77**, 394 (2000).

³G. von Freymann, U. Neuberth, M. Deubel, M. Wegener, G. Khitrova, and H.M. Gibbs, *Phys. Rev. B* **65**, 205327 (2002).

⁴U. Neuberth, L. Walter, G. von Freymann, Th. Schimmel, M. Wegener, G. Khitrova, and H.M. Gibbs, *Appl. Phys. Lett.* **81**, 1881 (2002).

⁵A. Crottini, R.I. Kaitouni, J.L. Staehli, B. Deveaud, X.L. Wang, and M. Ogura, *Phys. Status Solidi A* **190**, 631 (2002).

⁶Y. Yayon, A. Esser, M. Rappaport, V. Umansky, H. Shtrikman, and I. Bar-Joseph, *Phys. Rev. Lett.* **89**, 157402 (2002).

⁷V. Savona, S. Haacke, and B. Deveaud, *Phys. Rev. Lett.* **84**, 183 (2000).

⁸E. Runge and R. Zimmermann, *Adv. Solid State Phys.* **38**, 251 (1998).

⁹V. Savona and R. Zimmermann, *Phys. Rev. B* **60**, 4928 (1999).

¹⁰For a recent overview, see T. Guhr, A. Müller-Groeling, and H.A. Weidenmüller, *Phys. Rep.* **299**, 190 (1998).

¹¹R. Zimmermann, F. Große, and E. Runge, *Pure Appl. Chem.* **69**, 1179 (1997).

¹²E. Runge, *Excitons in Semiconductor Nanostructures*, Solid State Physics, Vol. 57, edited by H. Ehrenreich and F. Spaepen (Academic Press, San Diego, 2002), pp. 149–305.

¹³J.R. Guest, T.H. Stievater, D.G. Steel, D. Gammon, D.S. Katzer, and D. Park, Quantum Electronics and Laser Science Conference, OSA Technical Digest (2000), p. 6.

¹⁴D. Gammon, E.S. Snow, B.V. Shanabrook, D.S. Katzer, and D. Park, *Phys. Rev. Lett.* **76**, 3005 (1996).

¹⁵N.H. Bonadeo, J. Erland, D. Gammon, D. Park, D.S. Katzer, and D.G. Steel, *Science* **282**, 1473 (1998).

¹⁶C.A. Warwick, W.Y. Jan, A. Ourmazd, and T.D. Harris, *Appl. Phys. Lett.* **56**, 2666 (1990).

¹⁷R. Nötzel, M. Ramsteiner, J. Menniger, A. Trampert, H.-P. Schönherr, L. Däweritz, and K.H. Ploog, *Jpn. J. Appl. Phys.* **35**, L297 (1996).

¹⁸A. Richter, G. Behme, M. Süptitz, C. Lienau, T. Elsaesser, M. Ramsteiner, R. Nötzel, and K.H. Ploog, *Phys. Rev. Lett.* **79**, 2145 (1997).

¹⁹V. Emiliani, T. Guenther, C. Lienau, R. Nötzel, and K.H. Ploog, *Phys. Rev. B* **61**, R10583 (2000).

²⁰F. Intonti, V. Emiliani, C. Lienau, T. Elsaesser, R. Nötzel, and K.H. Ploog, *Phys. Rev. B* **63**, 075313 (2001).

²¹K. Brunner, G. Abstreiter, G. Böhm, G. Tränkle, and G. Weimann, *Phys. Rev. Lett.* **73**, 1138 (1994).

²²A. Hartmann, Y. Ducommun, E. Kapon, U. Hohenester, and E. Molinari, *Phys. Rev. Lett.* **84**, 5648 (2000).

²³Q. Wu, R.D. Grober, D. Gammon, and D.S. Katzer, *Phys. Rev. B* **62**, 13022 (2000).

²⁴U. Neuberth, L. Walter, G. von Freymann, B. Dal Don, H. Kalt, M. Wegener, G. Khitrova, and H.M. Gibbs, *Appl. Phys. Lett.* **80**, 3340 (2002).

- ²⁵E. Runge and R. Zimmermann, *Phys. Status Solidi B* **206**, 167 (1998).
- ²⁶A. Feltrin, R. Idrissi Kaitouni, A. Crottini, J.L. Staehli, B. Deveaud, V. Savona, X.L. Wang, and M. Ogura, *Phys. Status Solidi C* **0**, 1417 (2003).
- ²⁷T. Guenther, C. Lienau, T. Elsaesser, M. Glanemann, V.M. Axt, T. Kuhn, S. Eshlaghi, and A.D. Wieck, *Phys. Rev. Lett.* **89**, 057401 (2002).
- ²⁸R. Zimmermann, E. Runge, and V. Savona, *Phys. Status Solidi B* **238**, 478 (2003).
- ²⁹ $R_c^{(\text{class})}(\Delta E)$ is simulated by generating N random realizations of the disorder potential $V_n(x_i, y_j)$ on the grid (x_i, y_j) , taking the eigenvalues $\epsilon_{i,j,n}$ as $V_n(x_i, y_j)$ and calculating local spectra $Dc_n(E) = \sum_{i,j} \delta(E - \epsilon_{i,j,n})$. Filter functions are then applied to $Dc_n(E)$.
- ³⁰Monolayer islands $V(\mathbf{R})$ can, e.g., be generated in two-dimensional simulations starting with a statistical disorder potential $\tilde{V}(\mathbf{R})$ with a large correlation length ξ and $\langle \tilde{V}(\mathbf{R}) \rangle = 0$ and choosing $V(\mathbf{R}) = +0.5 \cdot E_{ML}$ if $\tilde{V}(\mathbf{R}) > \alpha$ and $V(\mathbf{R}) = -0.5 \cdot E_{ML}$ if $\tilde{V}(\mathbf{R}) < \alpha$, with a small parameter α describing a possible asymmetry between narrow and wide well regions. Here, E_{ML} denotes the monolayer energy. Additional assumptions might be needed to obtain the narrow spread of features sizes suggested by the experiments.
- ³¹J.R. Guest, T.H. Stievater, X. Li, J. Cheng, D.G. Steel, D. Gammon, D.S. Katzer, D. Park, C. Ell, A. Thränhardt, G. Khitrova, and H.M. Gibbs, *Phys. Rev. B* **65**, 241310(R) (2002).
- ³²M. Wassermeier, J. Sudijono, M.D. Johnson, K.T. Leung, B.G. Orr, L. Däweritz, and K. Ploog, *Phys. Rev. B* **51**, 14721 (1995).